Accurate 3-dimensional Image Expansion Algorithm using Range Derivative of Double Scattered Signals for UWB Radars

Shouhei Kidera and *Tetsuo Kirimoto*
Graduate School of Informatics and Engineering, University of Electro-Communications, Tokyo, Japan
Email: kidera@ee.uec.ac.jp

Abstract

UWB(Ultra Wideband) radar offers a high range resolution and has a great promise to the near field sensing system, such as robotic or security sensor, that can identify a target even in an optically harsh environment. In recent years, some of radar imaging algorithms proactively employing multiple scattered components have been developed, which can enhance an imaging range compared to that synthesized by a single scattered one. As such, we have already proposed the SAR (Synthetic Aperture Radar) method using double scattered signals, and it successfully expanded a reconstructible range of radar imagery without any preliminary knowledge of target or surroundings. However, it is based on the multiple integration of the received signals, that requires an intensive computation, and also its spatial resolution is generally insufficient for clear boundary extraction such as edge or specular surface. As a substantial solution for the above problems, this paper proposes a novel expanded 3-dimensional (3-D) imaging algorithm based on range derivatives of double scattered signals. Some results in numerical simulations verify that the proposed method remarkably enhances the visible range of radar imagery without any integration process, and extremely decreases the calculation amount compared to that of the conventional method.

1 Introduction

UWB pulse radar with high range resolution creates various applications for near field sensing. As such, a robotic sensor is one of the most promising applications, able to identify a human body even in optically blurry visions such as dark smog in disaster areas or high-density gas in resource exploration scenes. While various kinds of radar algorithms have been developed based on the an aperture synthesis [1], the time reversal approach [2] or the range migration [3], they are not suitable for the above applications because it is, generally, difficult to achieve both properties of low computation cost and high spatial resolution. As a high-speed and accurate imaging method feasible for complex-shaped targets, the RPM (Range Points Migration) algorithm has been established [4]. This algorithm directly estimates an accurate direction of arrival with the global characteristic of observed range points, avoiding the difficulty of connecting them. The RPM is based on a simple idea, yet, it offers accurate and super-resolution surface extraction even for an extremely complicated boundary. However, they all have the unresolvable problem that aperture size strictly constrains the imaging range of target boundary. In many cases, the greater part of a target shape, such as a side of the target, falls into a shadow region since only single scattered components are used for imaging.

To enhance imaging range, the SAR algorithm based on a double scattered path has been developed [5]. Although this method proves that the shadow region imaging is possible by positively using the double scattered signals without preliminary observations or target models, this method requires multiple integrations of the received signals, and incurs a large calculation cost. As a solution for these problems, this paper proposes a novel imaging algorithm based on the range derivative of doubly scattered signals, where an initial image obtained by RPM is used to the best effect. This method is based on an original formula that each DOA of the double scattered points is strictly derived from the derivative of range points. This formula enables us to directly estimate a target boundary corresponding to the doubly scattered centers without any integration procedures. The result of numerical simulation, investigating toric and cylindrical objects, shows that this method accomplishes high-speed target boundary extraction, in situations which produce a shadow using the existing techniques.

2 System Model

The left hand side of Fig. 1 shows the system model. It assumes the mono-static radar, and an omni-directional antenna is scanned on $z = 0$ plane. It is assumed that the target has an arbitrary shape with a clear boundary. The propagation speed of the radio wave c is assumed to be a known constant. A mono-cycle pulse is used as the transmitting current. The real space in which the target and antenna are located, is

978-1-4244-6051-9/11/$26.00 ©2011 IEEE

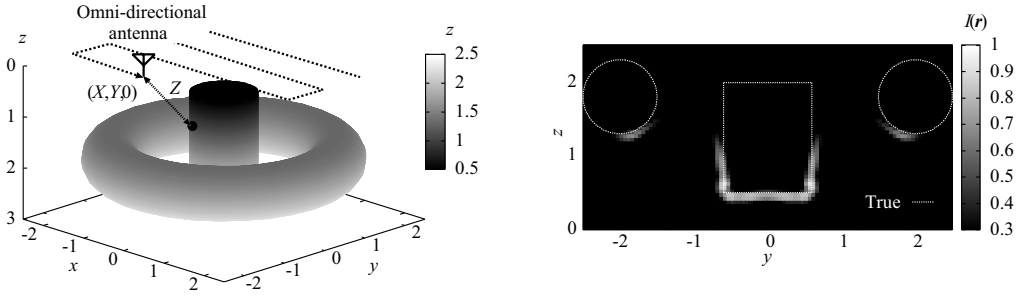

Figure 1: System model (left). The estimated image $I(\boldsymbol{r})$ with the conventional method at $x = 0$ (right).

expressed by the parameters (x, y, z). The parameters are normalized by λ, which is the central wavelength of the pulse. $z > 0$ is assumed for simplicity. $s'(X, Y, Z)$ is defined as the received electric field at the antenna location $(x, y, z) = (X, Y, 0) \equiv \boldsymbol{p}_L$, where $Z = ct/(2\lambda)$ is a function of time t. $s(X, Y, Z)$ is defined as the output of the Wiener filter with the transmitted waveform. This procedure is detailed in [4].

3 Conventional Method

As the conventional approach for enhancing the imaging range, the SAR employing the double scattered signal has been already developed [5]. In general, a double scattered wave propagates with a different path from that of a single scattered one. It therefore often provides independent information as to the two scattering points. This method synthesizes the additional image $I_2(\boldsymbol{r})$ for $\boldsymbol{r} = (x, y, z)$, considering a double scattered path,

$$I_2(\boldsymbol{r}) = -\int_{\boldsymbol{r'} \in R} \int_{\boldsymbol{p}_L \in \Gamma} I_1(\boldsymbol{r}') s\left(\boldsymbol{p}_L, d_2(\boldsymbol{r}, \boldsymbol{r}', \boldsymbol{p}_L)/2\right) \mathrm{d}X \mathrm{d}Y \ \mathrm{d}\boldsymbol{r}', \tag{1}$$

where $\boldsymbol{r'} = (x', y', z')$, R denotes the spatial region for image reconstruction, Γ is observation range, and $d_2(\boldsymbol{r}, \boldsymbol{r'}, \boldsymbol{p}_L) = \|\boldsymbol{r} - \boldsymbol{p}_L\| + \|\boldsymbol{r}' - \boldsymbol{p}_L\| + \|\boldsymbol{r} - \boldsymbol{r}'\|$ holds. $I_1(\boldsymbol{r})$ denotes the original SAR image. The minus sign in Eq. (1) creates a positive image focused by double scattered waves that have an antiphase relationship from a single scattered one. The final image is defined as $I(\boldsymbol{r}) = I_1(\boldsymbol{r}) H\left(I_1(\boldsymbol{r})\right) / \{\max_{\boldsymbol{r}} I_1(\boldsymbol{r})\} + I_2(\boldsymbol{r}) H\left(I_2(\boldsymbol{r})\right) / \{\max_{\boldsymbol{r}} I_2(\boldsymbol{r})\}$, where $H(*)$ is the Heaviside function.

The left hand side of Fig. 1 shows the estimated image $I(\boldsymbol{r})$ at $x = 0$, where the target boundary as in the right hand side of Fig. 1 is assumed. The received signal is obtained at $-2.5 \leq x, y \leq 2.5$ using FDTD (Finite Difference Time Domain) method, where the number of locations on each axis is 101. This figure shows that the part of the side of the cylindrical target can be reproduced, and significantly expands the imaging range. The reason is that double scattered waves are effectively focused on the part of the target side using Eq. (1). It also claims that this method does not require target modeling or a priori information of the surroundings. However, it requires the fifth time integration for imaging and its calculation time goes up to over 10^6 sec for an Intel Pentium D 2.8 GHz processor.

4 Proposed Method

To overcome the problems described in the above, this paper proposes a high-speed 3-D imaging algorithm for the shadow region based on a novel approach. This method employs target points preliminarily created by the RPM method [4], and accurately reconstructs the target points corresponding to the double scattered signals with their range derivatives.

First, a basic theory of the proposed method is described below. Here, two target points originating from doubly scattering are defined as $\boldsymbol{p}_i \equiv (x_i, y_i, z_i) = \boldsymbol{p}_L + (Z_i \cos\theta_i \cos\phi_i, Z_i \sin\theta_i \cos\phi_i, Z_i \sin\phi_i)$, $(i = 1, 2)$, where $Z_1 = \|\boldsymbol{p}_1 - \boldsymbol{p}_L\|$, $Z_2 = \|\boldsymbol{p}_2 - \boldsymbol{p}_L\|$, $0 \leq \theta_1, \theta_2 < 2\pi$ and $0 < \phi_1, \phi_2 \leq \pi/2$ hold. The left hand side of Fig. 2 shows the example for $\boldsymbol{p}_1$, $\boldsymbol{p}_2$ and $\boldsymbol{p}_L$. (X, Y, Z_D) is defined as a range point of double scattered wave, which is extracted from the local minimum of $s(X, Y, Z)$. Here, if $\partial Z_D/\partial X$ and $\partial Z_D/\partial Y$ exist on

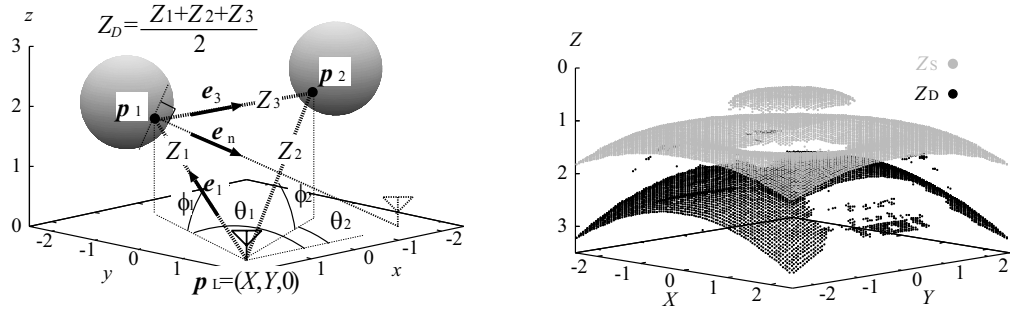

Figure 2: The relationship among $\boldsymbol{p}_1$, $\boldsymbol{p}_2$ and $\boldsymbol{p}_L$ (left). The extracted range points of single (gray) and double (black) scattered signals for targets in the left hand side of Fig. 1 (right).

each (X, Y, Z_D), the next formulae hold,

$$\left.\begin{aligned} \frac{\partial Z_D}{\partial X} &= \frac{\cos\theta_1\cos\phi_1 + \cos\theta_2\cos\phi_2}{2} \\ \frac{\partial Z_D}{\partial Y} &= \frac{\sin\theta_1\cos\phi_1 + \sin\theta_2\cos\phi_2}{2} \end{aligned}\right\}. \tag{2}$$

Then, once $\boldsymbol{p}_1$ is determined, ϕ_2 and θ_2 are readily calculated from $(\partial Z_D/\partial X, \partial Z_D/\partial Y)$ in Eq. (2). Besides, if the normal vector $\boldsymbol{e}_{\rm n}$ on $\boldsymbol{p}_1$ is given, the law of reflection derives Z_2,

$$Z_2 = Z_D - Z_1\frac{(Z_D - Z_1)(\boldsymbol{e}_1\cdot\boldsymbol{e}_{\rm n})^2}{Z_D - Z_1(\boldsymbol{e}_1\cdot\boldsymbol{e}_{\rm n})^2} \tag{3}$$

where $\boldsymbol{e}_1 = (\boldsymbol{p}_1 - \boldsymbol{p}_L)/Z_1$ holds. Thus, $\boldsymbol{p}_2$ can be calculated from $\boldsymbol{p}_1$ and $\boldsymbol{e}_{\rm n}$ in Eqs. (2) and (3). Furthermore, $\boldsymbol{p}_2$ satisfies $\boldsymbol{p}_2 = \boldsymbol{p}_1 + Z_3\boldsymbol{e}_3$, where $Z_3 \equiv \|\boldsymbol{p}_2 - \boldsymbol{p}_1\| = 2Z_D - Z_1 - Z_2$ and $\boldsymbol{e}_3 = \boldsymbol{e}_1 - 2(\boldsymbol{e}_{\rm n}\cdot\boldsymbol{e}_1)\boldsymbol{e}_{\rm n}$.

Second, the proposed method makes uses of the preliminary estimated target points by RPM as the first scattering location $\boldsymbol{p}_1$ with its normal vector $\boldsymbol{e}_{\rm n}$. RPM basically converts the range points to the target points, satisfying an one-to-one correspondence. Here, we define each target and range point with the RPM as $\boldsymbol{p}_i^{\rm rpm} \equiv (x_i^{\rm rpm}, y_i^{\rm rpm}, z_i^{\rm rpm})$ and $\boldsymbol{q}_i^{\rm rpm} \equiv (X_i^{\rm rpm}, Y_i^{\rm rpm}, Z_i^{\rm rpm})$, $(i = 1, \cdots N_{\rm T}^{\rm rpm})$, where $N_{\rm T}^{\rm rpm}$ is the total number of target points by RPM. In addition, each normal vector $\boldsymbol{e}_{{\rm n},i}^{\rm rpm}$ on $\boldsymbol{p}_i^{\rm rpm}$ is given as $\boldsymbol{e}_{{\rm n},i}^{\rm rpm} = \dfrac{(X_i^{\rm rpm} - x_i^{\rm rpm}, Y_i^{\rm rpm} - y_i^{\rm rpm}, -z_i^{\rm rpm})}{Z_i^{\rm rpm}}$. This relationship is derived from the assumption that each antenna receives a strong echo from the target boundary [4], which is perpendicular to a direction for a line of sight as shown in the left hand side of Fig. 2. This algorithm determines an optimal $\boldsymbol{p}_1$ from a set of the target points obtained by RPM, defined as $\mathcal{T}_{\rm rpm} = \left\{(x,y,z) \in \bigcup_{i=1}^{N_{\rm T}^{\rm rpm}} \boldsymbol{p}_i^{\rm rpm}\right\}$. Here, the parameter vector $\boldsymbol{P}_i$ is introduced as $\boldsymbol{P}_i \equiv (\boldsymbol{R}_i^{\rm rpm}; \boldsymbol{Q}_D)$, where $\boldsymbol{Q}_D \equiv (\boldsymbol{p}_L, Z_D, \partial Z_D/\partial X, \partial Z_D/\partial Y)$ $\boldsymbol{R}_i^{\rm rpm} \equiv (\boldsymbol{p}_i^{\rm rpm}, \boldsymbol{q}_i^{\rm rpm})$ hold. Then, the proposed method determines the optimum candidate $\hat{\boldsymbol{p}_1}$ for each $\boldsymbol{Q}_D$ as

$$\hat{\boldsymbol{p}_1}(\boldsymbol{Q}_D) = \underset{\boldsymbol{p}_i^{\rm rpm}\in\mathcal{T}_{\rm RPM}}{\arg\min} \left\|\boldsymbol{p}_2^A(\boldsymbol{P}_i) - \boldsymbol{p}_2^B(\boldsymbol{P}_i)\right\|^2, \tag{4}$$

where, $\boldsymbol{p}_2^A(\boldsymbol{P}_i) \equiv \boldsymbol{p}_L + (Z_2(\boldsymbol{P}_i)\cos\theta_2(\boldsymbol{P}_i)\cos\phi_2(\boldsymbol{P}_i), Z_2(\boldsymbol{P}_i)\sin\theta_2(\boldsymbol{P}_i)\cos\phi_2(\boldsymbol{P}_i), Z_2\sin\phi_2(\boldsymbol{P}_i))$, and $\boldsymbol{p}_2^B(\boldsymbol{P}_i) \equiv \boldsymbol{p}_i^{\rm rpm} + Z_3(\boldsymbol{P}_i)\boldsymbol{e}_{3,i}^{\rm rpm}$ hold. The optimum second scattering point $\hat{\boldsymbol{p}_2}(\boldsymbol{Q}_D)$ is determined as $\hat{\boldsymbol{p}_2}(\boldsymbol{Q}_D) = \left(\boldsymbol{p}_2^A(\hat{\boldsymbol{P}}) + \boldsymbol{p}_2^B(\hat{\boldsymbol{P}})\right)/2$, where $\hat{\boldsymbol{P}}$ is defined as $\boldsymbol{P}_i$ when the evaluation value in the right term in Eq. (4) becomes minimum. Note that, this method does not employ any integration of the scattered signals and directly determines the doubly scattering points using the derivative of the range points.

5 Performance Evaluation in Numerical Simulation

This section investigates the imaging performance for each method in a numerical simulation. The assumed target boundary and the received signals are same as in the case investigated in Sec. 3. The right hand side of Fig. 2 shows the range points as (X, Y, Z_S) and (X, Y, Z_D) extracted from the output of a

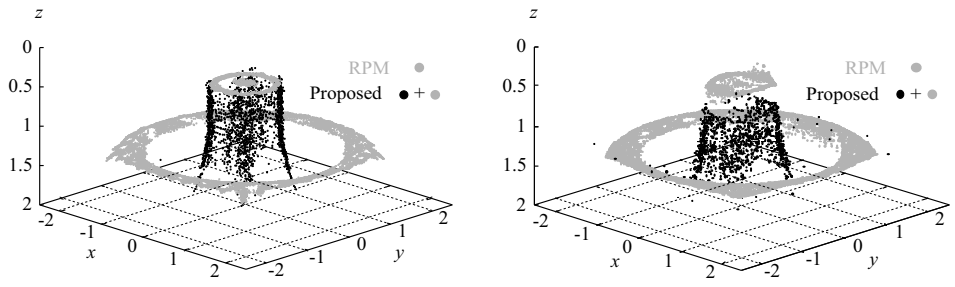

Figure 3: Estimated image with the proposed method in noiseless case (left) and in the case at S/N=30 dB (right).

Wiener filter in this case. The left hand side of Fig. 3 depicts the estimated 3-D image with the RPM and the proposed method. Here, $(\partial Z_D/\partial X, \partial Z_D/\partial Y)$ is calculated by the Gaussian smoothing to suppress fluctuations due to interference or noisy components. This figure verifies that the reconstructed target points express a quite accurate target boundary including the side of the cylindrical objects. This is because the double scattered wave propagates along the side of the toric and cylindrical boundaries. The mean accuracy of the estimated points is $2.80 \times 10^{-2}\lambda$ in this case. Note that, the proposed method requires only 10 sec for obtaining a full 3-D image after creating the target points with RPM. This amount is prominently reduced from that of the conventional method based on the fifth times integral for imaging after SAR processing [5], requiring around 10^6 sec. Moreover, this method creates the target points, not the intensified SAR image, which contributes to the identification of the edge or wedge region.

Finally, the example in noisy situation is investigated, whereby white Gaussian noise is added to each received signal as $s'(X, Y, Z)$. The right hand side of Fig. 3 shows the estimated points obtained by the proposed method, where the mean S/N is 30 dB. S/N is defined as the ratio of peak instantaneous signal power to the averaged noise power after applying the matched filter with the transmitted waveform. Although the mean accuracy of the estimated target points denoting $3.02 \times 10^{-2}\lambda$ distorts due to the false range points extracted from noisy components, the whole image can offer a significant target boundary including the side of the rectangular boundary.

6 Conclusion

This paper proposed a novel imaging algorithm for expanding the imaging range, which efficiently utilizes the range derivative of double scattered waves. This method has an outstanding advantage that it accomplishes extremely high-speed imaging by specifying a clear boundary extraction, simultaneously extending the visible region without any preliminarily knowledge of target or surroundings. Numerical simulations in the 3-D models, including multiple objects have shown that the proposed method substantially extended the imaging range holding the accuracy around $10^{-2}\lambda$. Particular to calculation time, it is a more than 10^5 times improvement compared with that of the conventional SAR based method. Thus, this method can significantly contribute to the design of real-time imaging sensors, as found in robots or security systems.

References

[1] D. L. Mensa, G. Heidbreder and G. Wade, "Aperture Synthesis by Object Rotation in Coherent Imaging," *IEEE Trans. Nuclear Science.*, vol. 27, no. 2, pp. 989–998, Apr, 1980.

[2] D. Liu, *et. al.*, "Electromagnetic Target Detection in Uncertain Media: Time-Reversal and Minimum-Variance Algorithms," *IEEE Trans. Geosci. Remote Sens.*, vol.45, no.4, pp. 934–944, Apr, 2007.

[3] F. Soldovieri, *et. al.*, "A Kirchhoff-Based Shape Reconstruction Algorithm for the Multimonostatic Configuration, " *IEEE Trans. Geosci. Remote Sens.*, vol. 46, no. 10, pp. 3031–3038, Oct, 2008

[4] S. Kidera, T. Sakamoto and T. Sato, "Accurate UWB Radar 3-D Imaging Algorithm for Complex Boundary without Range Points Connections," *IEEE Trans. Geosci. Remote Sens.*, vol. 48, no. 4, pp. 1993-2004, Apr., 2010.

[5] S. Kidera, T. Sakamoto and T. Sato, "Experimental Study of Shadow Region Imaging Algorithm with Multiple Scattered Waves for UWB Radars," *Proc. of PIERS*, Vol. 5, No. 4, pp. 393–396, Aug, 2009.